





Cite this: *Chem. Commun.*, 2024, 60, 4826

Received 4th January 2024,  
Accepted 2nd April 2024

DOI: 10.1039/d3cc06336d

rsc.li/chemcomm

# Kinetic isotope effect offers selectivity in CO<sub>2</sub> reduction†

Suman Patra,‡ Sayan Atta,‡ Soumili Ghosh, Amit Majumdar \* and  
Abhishek Dey \*

**A binuclear Ni complex with N,O donors catalyzes CO<sub>2</sub> reduction via its Ni(II) state. The product distribution when H<sub>2</sub>O is used as a proton source shows similar yields for CO, HCOOH and H<sub>2</sub>. However, when D<sub>2</sub>O is used, the product distribution shows a ~65% selectivity for HCOOH. *In situ* FTIR indicates that the reaction involves a Ni–COO\* and a Ni–CO intermediate. Differences in H/D KIEs on different protonation pathways determine the selectivity of CO<sub>2</sub> reduction.**

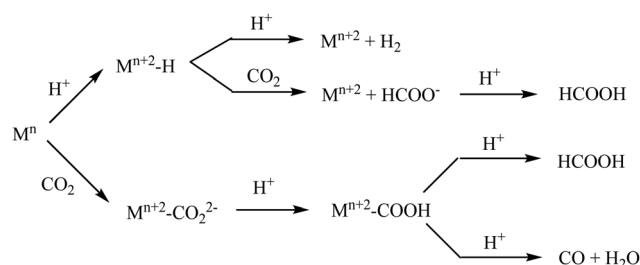
The reduction of CO<sub>2</sub> to chemicals having commercial value has taken centre stage in multi-electron multi-proton catalysis. Apart from the obvious appeal of the chemical conversion of a greenhouse gas to value added chemicals, the inherent challenges in the reaction have attracted the attention of several research groups across the world. Substantial progress has been made in the last few years and several molecular and material catalysts have been developed for this purpose and several of these show considerable reactivity.<sup>1–14</sup>

Reduction of CO<sub>2</sub> selectively to any of the several possible products poses a challenge. The 2e<sup>−</sup>/2H<sup>+</sup> reduction of CO<sub>2</sub> can produce either HCOOH or CO and competes with the reduction of protons to form H<sub>2</sub>.<sup>15–20</sup> Several groups have contributed to the current understanding of the mechanism of the reactions involved.<sup>8,21–26</sup> The reduced metal centre binds either CO<sub>2</sub> or H<sup>+</sup> to produce M–CO<sub>2</sub> or M–H species (Scheme 1). The M–H species can be further protonated to generate H<sub>2</sub> or it can transfer the H<sup>−</sup> to CO<sub>2</sub> to generate formate. The M–CO<sub>2</sub> species on the other hand generates a M–COOH species upon protonation and then can undergo either a M–C bond cleavage to generate formate or a C–O bond cleavage to generate CO. These species have been observed

chemically as well as by using spectro-electrochemistry and characterized.<sup>6,20,27</sup>

Selectivity in 2e<sup>−</sup>/2H<sup>+</sup> reduction has been demonstrated by several groups and it has been proposed that the electronic structure of the M–COOH species plays a vital role in the process.<sup>26</sup> When the M–C bond is very covalent, the protonation of the OH-group is favored resulting in C–O bond cleavage and release of CO, while in cases where the M–C bond is not very covalent, the M–C bond cleaves generating HCOOH. The covalency of the M–C bond can be tuned by the choice of the metal as well as the spin states. Using a ligand that has a protonation site has provided relief from the competing HER.<sup>20,28,29</sup>

In addition to the design of the ligand and the choice of metal controlling the electronic structure of the catalyst, selectivity can also be accessed by kinetic control. For example, at lower concentrations of protons (as well as by using weaker proton sources), the HER is naturally suppressed. In a curious case, the product distribution of 2e<sup>−</sup>/2H<sup>+</sup> CO<sub>2</sub> reduction by Pd/C was demonstrated to depend on the isotope of the proton source used. *In situ* X-ray characterization verifies the formation of Pd–H species. Substituting H<sub>2</sub>O with D<sub>2</sub>O reduces the rate of the competing hydrogen evolution reaction (HER) due to lower D<sup>+</sup> concentration and enhances the carbon dioxide reduction reaction (CO<sub>2</sub>RR), leading to a shift from 48% CO in H<sub>2</sub>O to 76% CO in D<sub>2</sub>O.<sup>30</sup> Clearly, the kinetic isotope effect (KIE) involved in the reduction of CO<sub>2</sub> was different from the KIE



**Scheme 1** Selectivity for 2e<sup>−</sup>/2H<sup>+</sup> reduction of CO<sub>2</sub> via the M–COOH pathway.

School of Chemical Sciences Indian Association for the Cultivation of Science 2A & 2B, Raja SC Mullick Road, Kolkata, WB 700032, India. E-mail: icam@iacs.res.in, abbeyde@gmail.com

† Electronic supplementary information (ESI) available: experimental details, control electrochemical experiments and structural data. CCDC 2208720 and 2310122. For ESI and crystallographic data in CIF or other electronic format see DOI: <https://doi.org/10.1039/d3cc06336d>

‡ These authors contributed equally.

involved in the reduction of  $\text{H}^+$  leading to different selectivities in  $\text{H}_2\text{O}$  and  $\text{D}_2\text{O}$ . Similar changes in product distribution were observed during  $\text{CO}_2$  reduction by cobalt phthalocyanine immobilized on a coordinating polymer support.<sup>31</sup> A significant kinetic isotope effect (KIE) was reported for the decomposition of  $\text{HCOOH}$  to form  $\text{CO}_2$  and  $\text{H}_2$  by an Ir/Ru complex.<sup>32</sup> Another study of isotope-controlled selectivity by quantum tunneling results in different chemical reactivity of cyclopropylmethylcarbene.<sup>33</sup> While isotope effects have been reported in the kinetics of electrochemical  $\text{CO}_2$  reduction using molecular catalysts, changes in selectivity have not been reported and whether such changes in selectivity can be obtained in a molecular catalyst under homogeneous conditions are yet to be evaluated.

In this manuscript, we report the synthesis of a novel binuclear Ni catalyst,  $[(\text{Py}2\text{ald})_2\text{Ni}_2](\text{BPh}_4)_2$  (**1**( $\text{BPh}_4$ )<sub>2</sub>), and explores its application in  $\text{CO}_2$  reduction by using water as the proton source. The ligand, HPy2ald (3-[[Bis(2-pyridinylmethyl)amino]methyl]-2-hydroxybenzaldehyde), was synthesized following literature report.<sup>34</sup> The catalyst shows no selectivity for either CO or  $\text{HCOOH}$  and exhibits a competing HER in  $\text{H}_2\text{O}$ . However, in  $\text{D}_2\text{O}$  the catalyst exhibits 65% selectivity for  $\text{HCOOH}$ . *In situ* spectro-electrochemical FTIR provides insight into the mechanism of  $\text{CO}_2$  reduction.

Cyclic voltammetry (CV) measurements conducted with 0.5 mM **1**( $\text{BPh}_4$ )<sub>2</sub> in  $\text{N}_2$  saturated acetonitrile solution unveiled two closely positioned peaks at  $-1.82$  V and  $-2.05$  V vs.  $\text{Fc}^+/\text{Fc}^0$ , respectively (Fig. 1A and inset). To identify the associated reduction process, CV was conducted using the free ligand HPy2ald under identical conditions. It was observed that the peak at  $-2.05$  V vs.  $\text{Fc}^+/\text{Fc}^0$  is linked to ligand reduction, potentially involving the reduction of the aldehyde group. Supporting evidence for this transformation is found in corroborating Fourier-transform infrared spectroscopy coupled with spectro-electrochemistry (FTIR-SEC) data. For **1**( $\text{BPh}_4$ )<sub>2</sub>, when the working electrode is held at  $-2.05$  V vs.  $\text{Fc}^+/\text{Fc}^0$ , the peak corresponding to the  $-\text{CHO}$  group at  $1633\text{ cm}^{-1}$  diminishes (Fig. 2A, inset), signifying its reduction, while a new peak in the  $2500\text{--}2700\text{ cm}^{-1}$  range emerges, corresponding to the formation of the  $-\text{CH}_2\text{OH}$  group (Fig. 2A). More importantly, the

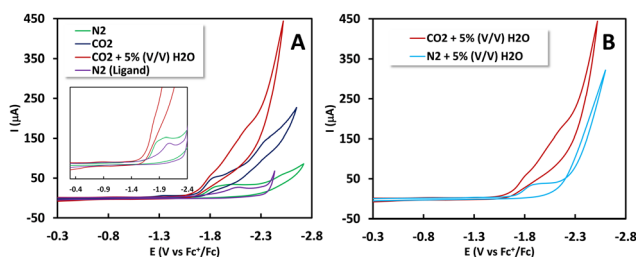


**Fig. 1** Cyclic voltammetry of 0.5 mM **1**( $\text{BPh}_4$ )<sub>2</sub> (green) and free ligand (purple trace) in  $\text{N}_2$  saturated acetonitrile solution, and its catalytic nature in  $\text{CO}_2$  saturated acetonitrile in the absence (blue trace) and presence of  $\text{H}_2\text{O}$  (red trace). The inset provides a zoomed-in view of the potential range from  $-0.4$  to  $-2.4$  V in an  $\text{N}_2$  atmosphere (A). Comparison of the CV trace of the Ni-complex in  $\text{CO}_2$  and  $\text{N}_2$  saturated acetonitrile in the presence of 5% (V/V)  $\text{H}_2\text{O}$  shows electrocatalytic  $\text{CO}_2$  reduction along with the HER (B). 100 mM tetrabutylammonium perchlorate (TBAP) was used as the supporting electrolyte.

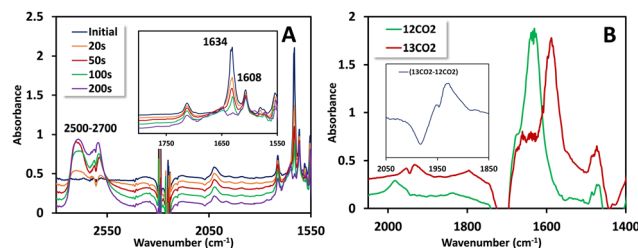


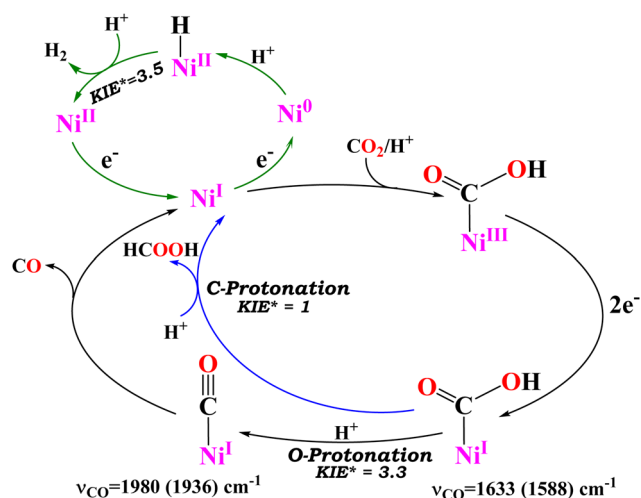
**Fig. 2** FTIR-SEC spectra of **1**( $\text{BPh}_4$ )<sub>2</sub> (4 mM) in  $\text{N}_2$  saturated acetonitrile while keeping the potential at  $-2.05$  V vs.  $\text{Fc}^+/\text{Fc}^0$  showing conversion of  $-\text{CHO}$  to  $-\text{CH}_2\text{OH}$ . The inset shows the zoomed-in view of the  $1550\text{--}1800\text{ cm}^{-1}$  region (A); *in situ* FTIR-SEC spectra (CPE at  $-2.2$  V vs.  $\text{Fc}^+/\text{Fc}^0$ ) of the intermediates of **1**( $\text{BPh}_4$ )<sub>2</sub> (4 mM) in acetonitrile using  $^{12}\text{CO}_2$  (blue trace) and  $^{13}\text{CO}_2$  (red trace) as substrates. The inset shows the zoomed-in difference spectra ( $^{13}\text{CO}_2\text{--}^{12}\text{CO}_2$ ) of the  $1850\text{--}2050\text{ cm}^{-1}$  region, showing a shift of  $44\text{ cm}^{-1}$  (B). 100 mM tetrabutylammonium perchlorate (TBAP) was used as the supporting electrolyte.

complete reduction of the  $-\text{CHO}$  vibration indicates that both  $-\text{CHO}$  groups are being reduced. The additional peak at  $-1.82$  V vs.  $\text{Fc}^+/\text{Fc}^0$  is associated with the  $\text{Ni}(\text{II/I})$  reduction. The reduction of  $\text{Ni}^{\text{II}}$  to  $\text{Ni}^{\text{I}}$  was confirmed by FTIR-SEC under one atmosphere CO (Fig. S6, ESI<sup>†</sup>).  $\text{Ni}^{\text{II}}$  does not bind CO, but when FTIR-SEC at  $-1.85$  V vs.  $\text{Fc}^+/\text{Fc}^0$  was conducted, a clear  $\text{Ni}^{\text{I}}\text{--CO}$  vibration at  $1980\text{ cm}^{-1}$  was observed. Similar carbonyl species were previously reported in a binuclear cobalt complex bridged by pyrazole.<sup>11</sup>

In the presence of saturated  $\text{CO}_2$  and 5% (V/V)  $\text{H}_2\text{O}$ , a strong reduction current is observed at  $-2.2$  V vs.  $\text{Fc}^+/\text{Fc}^0$  with a pre-catalytic feature at  $-1.65$  V vs.  $\text{Fc}^+/\text{Fc}^0$  which indicates  $\text{CO}_2$  binding to the reduced  $\text{Ni}^{\text{I}}$  (Fig. 1A). The electrocatalytic current at  $-2.2$  V vs.  $\text{Fc}^+/\text{Fc}^0$  is not observed in the absence of  $\text{CO}_2$  and represents electrocatalytic  $\text{CO}_2$  reduction (Fig. 1B). These observations lead to the conclusion that the species responsible for  $\text{CO}_2$  binding is  $\text{Ni}(\text{I})$  but the electrocatalysis proceeds after further reduction of  $\text{Ni}^{\text{III}}\text{--CO}_2^-/\text{Ni}^{\text{III}}\text{--COOH}$  (represented as  $\text{Ni}^{\text{III}}\text{--COO}^*$ ). In the presence of 5% (V/V)  $\text{H}_2\text{O}$  in an  $\text{N}_2$  atmosphere, a catalytic current is observed with an onset at  $-2.3$  V vs.  $\text{Fc}^+/\text{Fc}^0$ , indicating the occurrence of the hydrogen evolution reaction (HER). The absorption spectra of **1**( $\text{BPh}_4$ )<sub>2</sub> before and after CPE show an 18% reduction of the bridging phenolate to Ni charge transfer, not present in a monomer (Fig. S11 and S12, ESI<sup>†</sup>) after 30 minutes.

To delve into the reaction mechanism and identify the intermediates involved, FTIR-SEC was carried out in a  $\text{CO}_2$ -saturated acetonitrile solution in an OTTE cell. While keeping the working electrode at  $-2.2$  V vs.  $\text{Fc}^+/\text{Fc}^0$ , the FTIR-SEC results unveiled the presence of two isotope-sensitive vibrations associated with  $^{13}\text{CO}_2$  (Fig. 2B). A peak observed at  $1633\text{ cm}^{-1}$ , which corresponds to a  $\text{Ni}^{\text{I}}\text{--COO}^*$  intermediate, shifted to  $1588\text{ cm}^{-1}$  when a heavier isotope of  $\text{CO}_2$  ( $^{13}\text{CO}_2$ ) was used. Another peak at  $1980\text{ cm}^{-1}$  was also observed, corresponding to the  $\text{Ni}^{\text{I}}\text{--CO}$  species previously observed, which is a likely precursor to the carbon monoxide gas detected during the gas analysis. This peak shifted to  $1936\text{ cm}^{-1}$  when  $^{13}\text{CO}_2$  was used (Fig. 2B, inset). Based on these observations, a plausible mechanism is proposed (Scheme 2). Further evidence for the mechanism is marshalled from kinetic isotope effects discussed later.

Controlled potential electrolysis (CPE) was conducted using a glassy carbon electrode with a larger surface area ( $2\text{ cm}^2$ ) (Fig. 3A). After electrolysis of  $0.5\text{ mM}$  of  $1(\text{BPh}_4)_2$  in  $\text{CO}_2$  saturated acetonitrile solution in the presence of  $5\%$  (V/V)  $\text{H}_2\text{O}$ , the gaseous products generated were collected from the headspace and were subjected to analysis using gas chromatography (GC) equipped with a thermal conductivity detector (TCD). The GC-TCD analysis revealed the presence of two gases: hydrogen and carbon monoxide (Fig. 3B and Fig. S8, ESI<sup>†</sup>). The faradaic yields were determined to be  $32\%$  for hydrogen and  $23\%$  for carbon monoxide. An additional  $36\%$  of the product was identified as formate, when the solution, after electrolysis, was extracted with water and subsequently analysed by ion chromatography (Fig. 3C and Fig. S9, ESI<sup>†</sup>). Reduction of the metal may lead to formation of Ni nanoparticles on the electrode. The rinse test of the working electrode after CPE, however, does not show any catalytic activity (Fig. S10, ESI<sup>†</sup>). The results from the CPE indicate that  $1(\text{BPh}_4)_2$  exhibits no particular selectivity for either of the three  $2\text{e}^-/2\text{H}^+$  reduced products, *i.e.*  $\text{H}_2$ ,  $\text{CO}$  and  $\text{HCOOH}$  (Fig. 3D). The mechanistic pathway likely involved in  $2\text{e}^- \text{CO}_2$  reduction (Scheme 1) by  $1(\text{BPh}_4)_2$  would include key intermediates like  $\text{Ni-COOH}$  and  $\text{Ni-CO}$ . The  $\text{Ni-COOH}$  species would lead to  $\text{CO}$  after a C-O bond cleavage which upon protonation of the C-atom of the  $\text{Ni-COOH}$  species will release  $\text{HCOOH}$ . Formation of  $\text{H}_2$  entails protonation of the reduced Ni centre (Scheme 1) forming a  $\text{Ni-H}$  species. The same  $\text{Ni-H}$  species can produce  $\text{HCOOH}$  by reducing  $\text{CO}_2$  (Scheme 1). The different possible pathways involved may or may not involve protonation in the rate determining step (rds). A rds where protons are involved generally show the H/D KIE. In fact,  $\text{CO}_2$  reduction as well as the competing hydrogen evolution has been reported to exhibit H/D KIEs<sup>30,31,35–37</sup> and, in general, pathways involving metal hydrides exert substantial KIEs. The KIEs can both offer insight into the mechanism involved and result in changes in product distribution, *i.e.* selectivity.



**Scheme 2** Reaction mechanism of different pathways of  $\text{CO}_2/\text{CO}$  (black arrow) and  $\text{CO}_2/\text{HCOOH}$  (blue arrow) along with the HER (green arrow). The relative KIE ( $\text{KIE}^*$ ) is shown for all the reaction pathways.

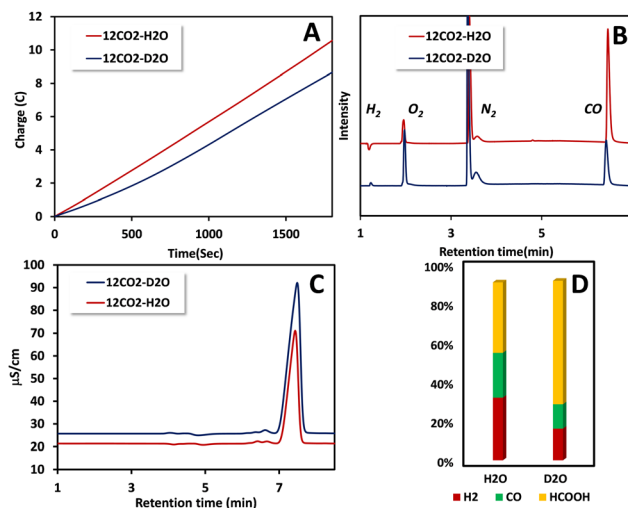


**Fig. 3** CPE performed at  $-2.2\text{ V}$  vs.  $\text{Fc}^+/\text{Fc}^0$  varying the heavier isotope of the proton source for  $1/2$  hour using a glassy carbon plate as the working electrode, Pt wire as the counter electrode and  $\text{Ag}/\text{AgCl}$  as the reference electrode. Charge consumption (A) followed by product detection using gas chromatography-TCD (B) and ion chromatography (C) and their faradaic yields (D) are compared for both  $\text{H}_2\text{O}$  and  $\text{D}_2\text{O}$  ( $^{12}\text{CO}_2/\text{H}_2\text{O}$  – red trace,  $^{12}\text{CO}_2/\text{D}_2\text{O}$  – blue trace).

In pursuit of a deeper understanding of the mechanism underlying carbon dioxide reduction, which yields both carbon monoxide and formic acid as reduced products, a kinetic isotope effect (KIE) investigation was undertaken. On using heavy water ( $\text{D}_2\text{O}$ ) instead of  $\text{H}_2\text{O}$ , the overall catalytic current was decreased (Fig. 3A). The products detected using GC and IC (ion chromatography) were  $\text{H}_2$ ,  $\text{CO}$  and  $\text{HCOOH}$ . However, the selectivity for  $\text{HCOOH}$  increases from  $36\%$  to a staggering  $63\%$  when  $\text{D}_2\text{O}$  is used instead of  $\text{H}_2\text{O}$ . The FY of  $\text{CO}$  and  $\text{H}_2$  shrinks from  $32\%$  and  $23\%$  to  $12\%$  and  $16\%$ , respectively. The charges consumed by  $\text{H}_2$ ,  $\text{CO}$  and  $\text{HCOOH}$  in  $\text{H}_2\text{O}$  were  $3.26\text{C}$ ,  $2.35\text{C}$  and  $3.67\text{C}$ , whereas in  $\text{D}_2\text{O}$  they were  $1.33\text{C}$ ,  $1.00\text{C}$  and  $5.23\text{C}$ , respectively (Table 1). Thus, in  $\text{D}_2\text{O}$  the production of  $\text{H}_2$  and  $\text{CO}$  is suppressed relative to  $\text{H}_2\text{O}$ , whereas the production of  $\text{HCOOH}$  is enhanced. These results present a unique case where the selectivity between the three products of CDR, namely  $\text{H}_2$ ,  $\text{CO}$  and  $\text{HCOOH}$ , for a molecular catalyst is shifted drastically by the use of isotopes.

The results indicate that  $\text{H}_2$  evolution and  $\text{CO}$  production are inhibited in the presence of  $\text{D}_2\text{O}$  relative to  $\text{H}_2\text{O}$ , while  $\text{HCOOH}$  production is accelerated. Since these reactions are competitive, the absolute currents being consumed cannot be used to derive a H/D KIE for the individual reactions. However, a relative KIE ( $\text{KIE}^*$  in Scheme 2) (Table 1) can be obtained relative to the  $\text{HCOOH}$  formation reaction. The reduction of  $\text{CO}_2$  to  $\text{CO}$  exhibits a relative KIE of  $3.3$ , while the  $\text{H}_2$  evolution shows a relative KIE of  $3.5$  relative to any implicit KIE  $\text{HCOOH}$  may have. Formation of  $\text{CO}$  requires two protons and it is likely that the second protonation step (protonation of the  $\text{M-COOH}$  species) is the rds, as suggested by its accumulation during catalysis, resulting in a H/D KIE. The relative KIE observed here is similar to the KIE observed in  $\text{CO}_2$  reduction to  $\text{CO}$  by

Table 1 Relative KIEs calculated for the three processes

Charge consumed	H <sub>2</sub> O		D <sub>2</sub> O		Relative KIE (H/D)
	10.2		8.3		
Products	Faradaic yield (%)	Charge (C)	Faradaic yield (%)	Charge (C)	
H <sub>2</sub>	32	3.26	16	1.33	3.5
CO	23	2.35	12	1.00	3.3
HCOOH	36	3.67	63	5.23	1

Co-thiolate complexes where the protonation of the –OH end of a M–COOH species is determined to be the rds.<sup>17</sup> Similarly, the formation of H<sub>2</sub> involves two protonation steps and the second protonation (*i.e.* protonation of M–H) is likely the rds that earns the H/D KIE. A similar KIE was recorded for H<sub>2</sub> evolution by Ni complexes where the protonation of the Ni–H species was the rds.<sup>38</sup>

The formic acid produced can be formed either *via* Ni–H attack on CO<sub>2</sub> or *via* C-protonation of the Ni–COOH intermediate. The H/D KIE reported for the hydride pathway is substantial (5–10)<sup>37</sup> because of the shift of the hydride from the metal to the CO<sub>2</sub> in the TS. The fact that the HCOOH increase in D<sub>2</sub>O contradicts this possibility in the case of 1(BPh<sub>4</sub>)<sub>2</sub>. Rather, the hydrolysis of Ni–COOH *via* C-protonation seems to be the most logical pathway.

In summary, differential H/D KIEs associated with the two competing 2e<sup>−</sup>/2H<sup>+</sup> CO<sub>2</sub> reduction pathways and that of the HER allow obtaining ~65% selectivity in HCOOH formation. This is the first example where selectivity in CO<sub>2</sub> reduction taking advantage of KIEs could be demonstrated in a molecular system.

The manuscript was written through contributions of all authors. All authors have given approval to the final version of the manuscript.

A. D. acknowledges SERB research grant no. CRG/2021/00154 and DST/TMD(EWO)/IC5-2018/03(G). A. M. acknowledges CRG/2022/001931 for funding. S. P., S. A., and S. G. acknowledge the CSIR for senior research fellowship.

## Conflicts of interest

There are no conflicts to declare.

## Notes and references

- 1 S. Overa, B. H. Ko, Y. Zhao and F. Jiao, *Acc. Chem. Res.*, 2022, **55**, 638–648.
- 2 J. Qiao, Y. Liu, F. Hong and J. Zhang, *Chem. Soc. Rev.*, 2014, **43**, 631–675.
- 3 H.-R. “Molly” Jhong, S. Ma and P. J. A. Kenis, *Curr. Opin. Chem. Eng.*, 2013, **2**, 191–199.
- 4 Q. Chang, Y. Liu, J.-H. Lee, D. Ologunagba, S. Hwang, Z. Xie, S. Kattel, J. H. Lee and J. G. Chen, *J. Am. Chem. Soc.*, 2022, **144**, 16131–16138.
- 5 H. Kang, A. Staples-West, A. Washington, C. Turchiano, A. Cooksy, J. Huang and J. Gu, *ChemCatChem*, 2023, **15**, e202300576.
- 6 A. J. Morris, G. J. Meyer and E. Fujita, *Acc. Chem. Res.*, 2009, **42**, 1983–1994.
- 7 R. Cao, *ChemSusChem*, 2022, **15**, e202201788.
- 8 S. Amanullah, P. Saha, A. Nayek, M. E. Ahmed and A. Dey, *Chem. Soc. Rev.*, 2021, **50**, 3755–3823.
- 9 S. Fang, M. Rahaman, J. Bharti, E. Reisner, M. Robert, G. A. Ozin and Y. H. Hu, *Nat. Rev. Methods Prim.*, 2023, **3**, 61.
- 10 M. Bonchio, J. Bonin, O. Ishitani, T.-B. Lu, T. Morikawa, A. J. Morris, E. Reisner, D. Sarkar, F. M. Toma and M. Robert, *Nat. Catal.*, 2023, **6**, 657–665.
- 11 A. Bohn, J. J. Moreno, P. Thuéry, M. Robert and O. Rivada-Wheelaghan, *Chem. – Eur. J.*, 2023, **29**, e202202361.
- 12 S. Amanullah, P. Gotico, M. Sircoglou, W. Leibl, M. J. Llansola-Portoles, T. Tibiletti, A. Quaranta, Z. Halime and A. Aukauloo, *Angew. Chem., Int. Ed.*, 2023, e202314439.
- 13 P. Gotico, Z. Halime, W. Leibl and A. Aukauloo, *ChemPlusChem*, 2023, **88**, e202300222.
- 14 C. Zhang, P. Gotico, R. Guillot, D. Dragoe, W. Leibl, Z. Halime and A. Aukauloo, *Angew. Chem., Int. Ed.*, 2023, **62**, e202214665.
- 15 L. Chen, Z. Guo, X.-G. Wei, C. Gallenkamp, J. Bonin, E. Anxolabéhère-Mallart, K.-C. Lau, T.-C. Lau and M. Robert, *J. Am. Chem. Soc.*, 2015, **137**, 10918–10921.
- 16 J. D. Froehlich and C. P. Kubiak, *Inorg. Chem.*, 2012, **51**, 3932–3934.
- 17 S. Dey, M. E. Ahmed and A. Dey, *Inorg. Chem.*, 2018, **57**, 5939–5947.
- 18 M. D. Sampson and C. P. Kubiak, *J. Am. Chem. Soc.*, 2016, **138**, 1386–1393.
- 19 C. G. Margarit, N. G. Asimow, C. Costentin and D. G. Nocera, *ACS Energy Lett.*, 2020, **5**, 72–78.
- 20 S. Amanullah, P. Saha and A. Dey, *J. Am. Chem. Soc.*, 2021, **143**, 13579–13592.
- 21 J. A. Barrett, C. J. Miller and C. P. Kubiak, *Trends Chem.*, 2021, **3**, 176–187.
- 22 C. Costentin, M. Robert and J.-M. Savéant, *Chem. Soc. Rev.*, 2013, **42**, 2423–2436.
- 23 Y. Yamazaki, H. Takeda and O. Ishitani, *J. Photochem. Photobiol., C*, 2015, **25**, 106–137.
- 24 E. Fujita, *Coord. Chem. Rev.*, 1999, **185–186**, 373–384.
- 25 E. Fujita, C. Creutz, N. Sutin and B. S. Brunswig, *Inorg. Chem.*, 1993, **32**, 2657–2662.
- 26 P. Saha, S. Amanullah and A. Dey, *Acc. Chem. Res.*, 2022, **55**, 134–144.
- 27 B. Mondal, A. Rana, P. Sen and A. Dey, *J. Am. Chem. Soc.*, 2015, **137**, 11214–11217.
- 28 A. Chapovetsky, M. Welborn, J. M. Luna, R. Haiges, T. F. I. I. Miller and S. C. Marinescu, *ACS Cent. Sci.*, 2018, **4**, 397–404.
- 29 M. E. Ahmed, A. Rana, R. Saha, S. Dey and A. Dey, *Inorg. Chem.*, 2020, **59**, 5292–5302.
- 30 J. H. Lee, B. M. Tackett, Z. Xie, S. Hwang and J. G. Chen, *Chem. Commun.*, 2020, **56**, 106–108.
- 31 Y. Liu and C. C. L. McCrory, *Nat. Commun.*, 2019, **10**, 1683.
- 32 S. Fukuzumi, T. Kobayashi and T. Suenobu, *J. Am. Chem. Soc.*, 2010, **132**, 1496–1497.
- 33 A. Nandi, D. Gerbig, P. R. Schreiner, W. T. Borden and S. Kozuch, *J. Am. Chem. Soc.*, 2017, **139**, 9097–9099.
- 34 I. A. Koval, D. Pursche, A. F. Stassen, P. Gamez, B. Krebs and J. Reedijk, *Eur. J. Inorg. Chem.*, 2003, 1669–1674.
- 35 N. Devi, C. K. Williams, A. Chaturvedi and J. “Jimmy” Jiang, *ACS Appl. Energy Mater.*, 2021, **4**, 3604–3611.
- 36 S. Dey, T. K. Todorova, M. Fontecave and V. Mougél, *Angew. Chem., Int. Ed.*, 2020, **59**, 15726–15733.
- 37 S. Roy, B. Sharma, J. Pécaut, P. Simon, M. Fontecave, P. D. Tran, E. Derat and V. Artero, *J. Am. Chem. Soc.*, 2017, **139**, 3685–3696.
- 38 D. Hong, Y. Tsukakoshi, H. Kotani, T. Ishizuka, K. Ohkubo, Y. Shiota, K. Yoshizawa, S. Fukuzumi and T. Kojima, *Inorg. Chem.*, 2018, **57**, 7180–7190.